Covariant energy density functionals: Nuclear matter constraints and global ground state properties

A. V. Afanasjev and S. E. Agbemava

Phys. Rev. C **93**, 054310 — Published 6 May 2016

DOI: 10.1103/PhysRevC.93.054310

Covariant energy density functionals: nuclear matter constraints and global ground state properties

A. V. Afanasjev[1] and S. E. Agbemava[1]

[1]*Department of Physics and Astronomy, Mississippi State University, MS 39762*

(Dated: April 21, 2016)

The correlations between global description of the ground state properties (binding energies, charge radii) and nuclear matter properties of the state-of-the-art covariant energy density functionals have been studied. It was concluded that the strict enforcement of the constraints on the nuclear matter properties (NMP) defined in Ref. [1] will not necessary lead to the functionals with good description of the binding energies and other ground and excited state properties. In addition, it will not substantially reduce the uncertainties in the predictions of the binding energies in neutron-rich systems. It turns out that the functionals, which come close to satisfying these NMP constraints, have some problems in the description of existing data. On the other hand, these problems are either absent or much smaller in the functionals which are carefully fitted to finite nuclei but which violate some NMP constraints. This is a consequence of the fact that the properties of finite nuclei are defined not only by nuclear matter properties but also by underlying shell effects. The mismatch of phenomenological content, existing in all modern functionals, related to nuclear matter physics and the physics of finite nuclei could also be responsible.

PACS numbers: 21.60.Jz, 21.10.Dr, 21.10.Ft, 21.10.Gv

I. INTRODUCTION

Bound states of the nucleons manifest themself in two species: finite nuclei and neutron stars. The former system is bound by strong forces, while the latter by gravitational ones. The description of both types of nuclear systems is intimately connected with a concept of nuclear matter which is an idealized infinite system of nucleons (neutrons and protons) interacting by strong forces. Infinite volume implies no surface effects and translational invariance. This concept is well suited for the description of the properties of interior of neutron stars.

However, it also has some important implications for finite nuclei (see Refs. [2–6] in recent topical review on nuclear symmetry energy). This is because the constraints on nuclear matter properties (NMP) enter into fitting protocols of the energy density functionals (EDF) for non-relativistic and covariant density functional theories [7, 8] (the abbreviation CDFT is used for latter one). In this way they affect the properties of finite nuclei (both static and dynamic aspects) [2–5, 7, 8].

The analysis of the 263 covariant energy density functionals (further CEDFs) with respect of NMP constraints has recently been performed in Ref. [1]. Note that only small portion of these functionals (less than 10) have been used in a more or less systematic studies of the properties of finite nuclei. The performance of other functionals with respect of the description of finite nuclei (apart of few spherical nuclei used in the fitting protocols) is not known. The properties of symmetric nuclear matter, pure neutron matter, symmetry energy and its derivatives were constrained based on experimental/empirical data and model calculations in Ref. [1]. This resulted in two sets of constraints called SET2a and SET2b relevant for CDFT models; the part of these constraints is listed in Table III below. Note that they are characterized by substantial uncertainties.

It turns out that among these 263 CEDFs only 4 and 3 satisfy SET2a and SET2b NMP constraints, respectively. However, these functionals have never been used in the studies of finite nuclei. Thus, it is impossible to verify whether good NMP of these functionals will translate into good global description of binding energies, charge radii, deformations etc. Removing isospin incompressibility constraint increases the number of functionals which satisfy SET2a and SET2b constraints to 35 and 30, respectively [1]. Again the performance of absolute majority of these functionals in finite nuclei is not known. However, among those are the FSUGold and DD-MEδ CEDFs the global performance of which has been studied in the RMF+BCS and RHB models in Refs. [9, 10], respectively. Additional constraints on the functionals come from the properties of neutron stars [11]. It turns out that FSUGold and DD-MEδ place maximum mass M of neutron star well below and above the measured limit of $1.93 \leq M/M_{\odot} \leq 2.05$ [12, 13] where $M_{\odot}$ is the solar mass. The DD-MEδ functional comes to this limit only when hyperons are included; however, there are substantial uncertainties in the meson-hyperon couplings [11] as well as in the existence of hyperons in the interior of neutron stars [14].

Thus, the number of questions emerge. First one is whether strict enforcement of these NMP constraints will inevitably lead to an improvement of the description of the ground state properties of finite nuclei in the CDFT and to a reduction of theoretical uncertainties in the description of the properties of neutron-rich nuclei. Another question is whether there is some physics missing in the current generation of CEDFs which could be responsible for some mismatch of the results for finite nuclei and neutron stars. It is also important to understand how the details of the fitting protocols affect these con-

clusions. The study of these questions represent the first goal of the present paper. The second goal is to understand whether future experimental data on the ground state properties of neutron-rich nuclei will allow to minimize theoretical uncertainties for physical observables of neutron-rich nuclei and to which extent. Such an approach assumes more reliance on the data on finite nuclei and less dependence on the NMP constraints in the definition of isovector properties of CEDFs.

To address these questions we perform the global analysis of the ground state observables such as binding energies and charge radii obtained with the state-of-the-art CEDFs which differ substantially in the NMPs. CEDF DD-MEδ, which is coming very close to satisfying all required NMP constraints, is among them. Binding energies of finite nuclei play an important role in the nuclear structure and nuclear astrophysics. Their evolution with charge and isospin defines the limits of nuclear landscape (Refs. [10, 15, 16]). Accurate modeling of nuclear astrophysics processes and the reduction of relevant theoretical uncertainties requires the precise knowledge of binding energies of neutron-rich nuclei which are currently non-accessible by experimental facilities [17].

The paper is organized as follows. Sec. II presents brief outline of theoretical framework. Theoretical uncertainties in the predictions of binding energies and the role of future experimental facilities in their reduction are discussed in Sec. III. Sec. IV considers the impact of nuclear matter properties of the functionals on the predictions of binding energies in known and neutron-rich nuclei. The accuracy of the description of the ground state properties of finite nuclei and its dependence on fitting protocol are discussed in Sec. V. Sec. VI is devoted to general observations following from this study. Finally, Sec. VII summarizes the results of our work.

II. BRIEF OUTLINE OF THE DETAILS OF THEORETICAL FRAMEWORK

The results have been obtained in the relativistic Hartree-Bogoliubov (RHB) framework the details of which are discussed in Secs. III and IV of Ref. [10]. These deformed RHB calculations are restricted to axial reflection symmetric shapes.

We focus on four CEDFs (NL3* [18], DD-ME2 [19], DD-PC1 [20] and DD-MEδ [21]) which were used in the global studies of Refs. [10, 16, 22] and for which numerical results are available. These functionals are compared in Sec. 2 of Ref. [10]. To deal with complete set of major classes of the state-of-the-art CEDFs, we also provide new results obtained with CEDF PC-PK1 [23] for the Yb isotope chain. This functional has been used with success for the studies of the masses of known nuclei by Peking group in Refs. [24, 25].

These functionals reproduce the binding energies of known nuclei at the mean field level with the rms-deviations of around 2.5 MeV (see Table II below). However, they differ substantially in the underlying physics (see discussion in Sec. 2 of Ref. [10] and Ref. [23]) and fitting protocols (see Table I and Fig. 5 below).

TABLE I. Input data for fitting protocols of different CEDFs. Columns (2-4) show the number of experimental data points on binding energies E, charge radii r_{ch} and neutron skin thicknesses r_{skin} used in the fitting protocols. Column 5 indicates which type of nuclei (spherical (S) or deformed (D)) were used. Column 6 shows whether microscopic equation of state (EOS) has been used in the fit of the functional or not; here "Y" stands for "yes" and "N" for "no".

CEDF	E	r_{ch}	r_{skin}	Type of nuclei	EOS
1	2	3	4	5	6
NL3*	12	9	4	S	N
DD-ME2	12	9	3	S	N
DD-MEδ	161	86	0	S	Y
DD-PC1	64	0	0	D	Y
PC-PK1	60	17	0	S	N

Table I shows that only two of these functionals, namely, DD-MEδ and DD-PC1, are fitted to the equation of state (EOS) of neutron matter obtained in microscopic calculations with realistic forces. Although these EOS are similar at saturation densities, they differ substantially in their stifness at the densities typical to the centre of neutron stars [3, 26, 27]. Note that no reliable data, either observational or experimental, exist for such densities. As a result, there is no way to discriminate these predictions for the EOS.

III. THEORETICAL UNCERTAINTIES IN THE PREDICTIONS OF BINDING ENERGIES AND THE ROLE OF FUTURE EXPERIMENTAL FACILITIES IN THEIR REDUCTION

The map of theoretical spreads $\Delta E(Z,N)$ in the predictions of the binding energies is shown in Fig. 1. These spreads are defined as

$$\Delta E(Z,N) = |E_{max}(Z,N) - E_{min}(Z,N)|, \qquad (1)$$

where $E_{max}(Z,N)$ and $E_{min}(Z,N)$ are the largest and the smallest binding energies for each (N,Z) nucleus obtained with four state-of-the-art functionals, namely, NL3*, DD-ME2, DD-MEδ and DD-PC1. Here the results of the calculations of Ref. [10], covering nuclear landscape between the two-proton and two-neutron drip lines, are used. The accuracy of the description of experimental masses by these functionals is given in Table II. Fig. 2a shows that the spreads in the predictions of binding energies stay within 5-6 MeV for the known nuclei (the regions with measured and measured+estimated masses[1] in Fig. 2a). These spreads are even smaller

[1] The masses given in the AME2012 mass evaluation [28] can be separated into two groups: One represents nuclei with masses

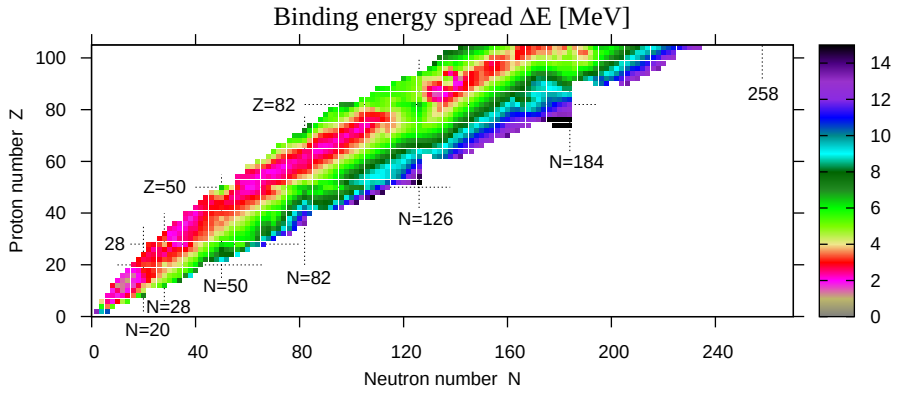

FIG. 1. (Color online) The binding energy spreads $\Delta E(Z,N)$ as a function of proton and neutron number. From Ref. [10].

TABLE II. The rms deviations ΔE_{rms} and $\Delta(r_{ch})_{rms}$ between calculated and experimental binding energies E and charge radii r_{ch}. The columns (2) and (4) show the ΔE_{rms} and $\Delta(r_{ch})_{rms}$ values obtained in the RHB calculations of Ref. [10] for the nuclei used in the fitting protocols of first four functionals. Note that our results for the DD-MEδ differ from the ones obtained in Ref. [21] which are shown in brackets. This is because 24 out of 161 nuclei used in the fit are deformed in our calculations; note that all these 161 nuclei were assumed to be spherical in Ref. [21]. The results for CEDF PC-PK1 are from Ref. [23]. The columns (3) and (5) show the ΔE_{rms} and $\Delta(r_{ch})_{rms}$ values obtained in global calculations. For first four functionals, they are defined in Ref. [10] with respect of 640 measured masses presented in the AME2012 compilation [28]. For PC-PK1 they are defined with respect of 575 masses in Ref. [24].

CEDF	ΔE^{fit}_{rms} [MeV]	ΔE^{global}_{rms} [MeV]	$\Delta(r_{ch})^{fit}_{rms}$[fm]	$\Delta(r_{ch})^{global}_{rms}$ [fm]
1	2	3	4	5
NL3*	1.68	2.96	0.017	0.0283
DD-ME2	1.48	2.39	0.015	0.0230
DD-MEδ	2.33 [2.4]	2.29	0.028 [0.02]	0.0329
DD-PC1	0.69	2.01	0.039[a]	0.0253
PC-PK1	1.33	2.58	0.019	

[a] Note that no information on charge radii has been used in the fit of the DD-PC1 CEDF [20].

(typically around 3 MeV) for the nuclei in the valley of beta-stability. However, theoretical uncertainties for the masses increase drastically when approaching the neutron-drip line and in some nuclei they reach 15 MeV. This is a consequence of poorly defined isovector properties of many CEDFs.

Fig. 2b shows the spreads of the relative errors in the predictions of binding energies which are defined as

$$\Delta E^{rel}(Z,N) = \frac{|E_{max}(Z,N) - E_{min}(Z,N)|}{\frac{1}{4}\sum_{i=1}^{4} E_i(Z,N)} \qquad (2)$$

where $E_i(Z,N)$ is the binding energy obtained with the i-th functional. The quantity in the denominator is the average binding energy of the (Z,N) nucleus obtained with four CEDFs. These spreads in relative errors are largest in light nuclei due to the effects which are not taken into account at the DFT level (see Ref. [10]). For known nuclei they gradually decrease with the increase of mass so that for the $A \geq 80$ nuclei the spreads in relative errors stay safely below 0.5%.

It is important to understand how future mass measurements with rare isotope facilities (such as FRIB, GANIL, RIKEN and FAIR) could help to improve isovector properties of the functionals. Fig. 2 clearly shows that the increase of the neutron number beyond the region of known nuclei leads to an increase of the ΔE and ΔE^{rel} spreads. However, apart of the $Z \sim 40, N \sim 82$ region these increases are quite modest in terms of binding energy spreads ΔE on going from currently known limit of neutron-rich nuclei (for which $\Delta E \sim 6$ MeV) up to the FRIB limit (for which $\Delta E \sim 8$ MeV). Note that for $Z \geq 70$ nuclei a similar transition almost does not increase the ΔE and ΔE^{rel} spreads. The largest increase in the ΔE spreads is observed in the $Z \sim 40$ nuclei for which the transition from the limit of currently known nuclei to the FRIB limit changes ΔE from ~ 6 MeV to ~ 12 MeV (Fig. 2a).

defined only from experimental data, the other contains nuclei with masses depending in addition on either interpolation or extrapolation procedures. For simplicity, we call the masses of the nuclei in the first and second groups as measured and estimated. There are 640 measured and 195 estimated masses of even-even nuclei in the AME2012 mass evaluation.

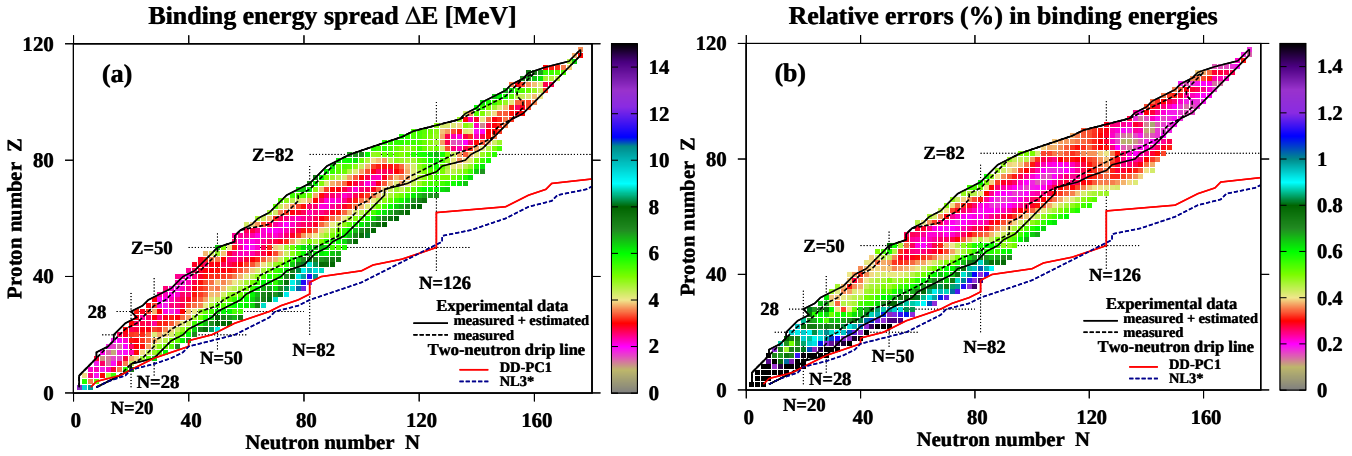

FIG. 2. (Color online) Panel (a) is based on the results presented in Fig. 1. However, the squares are shown only for the nuclei which are currently known and which will be measured with FRIB. The regions of the nuclei with measured and measured+estimated masses are enclosed by dashed and solid black lines, respectively. The squares beyond these regions indicate the nuclei which may be measured with FRIB. For simplicity the line formed by most neutron-rich nucleus in each isotope chain accessible with FRIB will be called as "FRIB limit". The FRIB limit of the nuclear chart is defined by fission yield greater than 10^{-6} that may be achieved with dedicated existence measurements [29]. The same colormap as in Fig. 1 is used here, but the ranges of particle numbers for vertical and horizontal axis are different from the ones in Fig. 1. The two-neutron drip lines are shown for the CEDFs NL3* and DD-PC1 by blue dashed and solid red lines, respectively. Panel (b) is based on the same results as panel (a), but the spreads in relative errors in the description of the masses are shown instead of binding energy spreads ΔE.

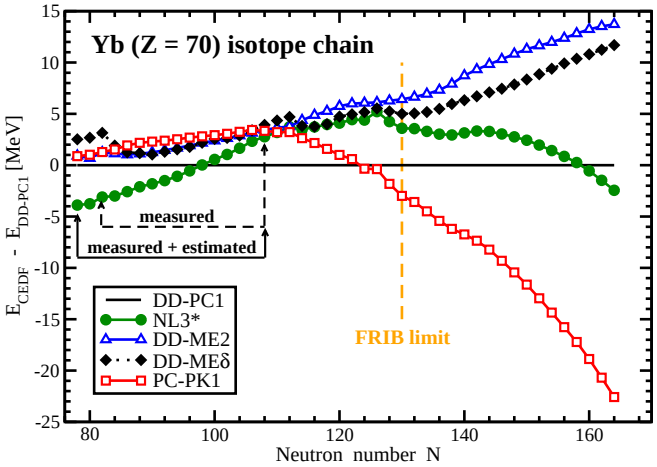

FIG. 3. (Color online) The differences in the calculated binding energies of the Yb nuclei obtained in the RHB calculations with two functionals. The results obtained with DD-PC1 are used as a reference. The regions of measured and measured+estimated masses from Ref. [28] are indicated by arrows. The FRIB limit is shown by dashed orange line.

These results suggest that new mass measurements with future rare isotope beam facilities, which (dependent on model) may reach two-neutron drip line or its vicinity for the $Z \leq 26$ nuclei (Fig. 2), could help to improve isovector properties of the CEDFs in the $Z \leq 50$ nuclei. However, this improvement is expected to be modest[2]. This is in part due to the fact that beyond mean field effects are quite important in light nuclei [10] which complicates the use of future data on masses for the refit of the functionals at the DFT level. The fact that the spread of relative errors in the predictions of the masses is the largest in light nuclei (see Fig. 2b) also underlines the fact that light nuclei are less "mean-field like" as compared with heavy ones. Even smaller improvement in the definition of isovector properties of the functionals is expected for the $50 \leq Z < 82$ nuclei since the increase in the ΔE spreads on going from the neutron-rich limit of the region of known nuclei to the FRIB limit is rather small being typically around 2 MeV or less. It is also clear that future rare isotope beam facilities will contribute very little to a better understanding of the isovector properties of the $Z \geq 82$ nuclei (Fig. 2).

The results presented in Figs. 1 and 2 are limited to the four CEDFs which were used in the global studies of Ref. [10]. In general, this group of CEDFs has to be supplemented by the PC-PK1 functional since then the set of the state-of-the-art functional representing major classes of CEDFs will be complete. This has not been done in Ref. [10] since the description of the ground state properties by PC-PK1 has been studied by the Peking group in the RMF+BCS framework in Ref. [24]. However, the properties of superheavy and octupole deformed nuclei

[2] This is in line with recent results of Ref. [30] which indicates that new mass measurements do not impose a strong enough constraint to generate significant changes in the energy density functionals.

have been studied globally with all five functionals in Refs. [31, 32].

We have not performed additional global studies with the PC-PK1 functional since the main conclusions can be derived based on the RHB results for the CEDFs NL3*, DD-ME2, DD-PC1 and DD-MEδ obtained earlier in Ref. [10]. However, we will illustrate the performance of this functional on the example of the Yb nuclei. The results for calculated binding energies are presented in Fig. 3. Here the results obtained with DD-PC1 are used as a reference since this functional provides the best description of the binding energies (see Table II and Fig. 6d below). In the region of known nuclei, the predictions of the PC-PK1 functional are very close to the ones obtained with the DD-ME2 and DD-MEδ functionals. With increasing neutron number N the PC-PK1 results come closer to those obtained with DD-PC1 and above $N = 122$ the nuclei are more bound in PC-PK1 than in DD-PC1. However, for the Yb nuclei within the FRIB limit (apart of the $N = 128, 130$ Yb isotopes), the spreads of binding energies ΔE presented in Figs. 1 and 2 would be only marginally affected by the addition of the results obtained with the PC-PK1 functional. On the other hand, the effect of addition of PC-PK1 on ΔE is very substantial for the nuclei beyond the FRIB limit where ΔE increases from ~ 16 MeV to ~ 37 MeV for $N = 162$ (see Fig. 3). These differences are caused by different isovector properties of CEDFs under study since calculated deformations are similar for all functionals. These results for ΔE are not surprising considering that even the functionals accurately fitted to the masses show substantial differences in the binding energies of neutron-rich nuclei. For example, the Skyrme functionals HFB-22 and HFB-24, which describe known masses with an accuracy of approximately 0.6 MeV [3], are characterized by the ΔE values reaching 10 MeV in neutron-rich nuclei (see Fig. 3 in [3]).

Note that there are some important similarities between the NL3* and PC-PK1 functionals. First, the evolution of the pairing energies and pairing gaps with neutron number in PC-PK1 is very similar to the one in NL3* (see Fig. 3 in Ref. [22] for the NL3* results). Second, both functionals predict the position of the two-neutron drip line at higher neutron number (at $N = 178$ for NL3* and at $N = 184$ for PC-PK1) as compared with the DD-* functionals with explicit density dependence which predict it at $N \sim 162$ (see Table IV in Ref. [10]).

IV. THE IMPACT OF NUCLEAR MATTER PROPERTIES OF THE FUNCTIONALS ON THE PREDICTIONS OF BINDING ENERGIES OF KNOWN AND NEUTRON-RICH NUCLEI

Although new experimental data on masses of neutron-rich nuclei generated by future rare isotope facilities will allow to improve the isovector properties of the energy density functionals, it is not likely that such an improvement will either eliminate or substantially reduce all possible uncertainties. Moreover, it is not clear whether the bias towards light and medium mass nuclei generated by future experimental data could be avoided since very little extension of the nuclear chart will be generated for the $Z \geq 82$ nuclei by these experiments (Fig. 2). This is precisely the region where most of unknown $Z \leq 120$ nuclei are located and where the distance (in terms of neutrons) between the region of known nuclei and the two-neutron drip line is the largest (see Fig. 1 in Ref. [16]).

The fitting protocols of EDFs always contain data on finite nuclei (typically binding energies, charge radii and occasionally neutron skin thicknesses) and pseudodata on NMP (see Table I and Sect. II in Ref. [10] for more details). Binding energies and radii show different sensitivity to various terms of the CEDFs and, in addition, there are some important correlations between the NMP and surface properties of the functionals. For example, the calculated binding energies are not very sensitive to the nuclear matter saturation density but are strongly influenced by the choice of the parameters which define the surface energy coefficient a_s in the empirical mass formula [20]. Strong converse relation exists between the nuclear charge radii and the saturation density of symmetric nuclear matter ρ_0 [33]. In addition, there is a strong correlation between the slope of symmetry energy L_0 and neutron skins [33–35] (see Refs. [33–37] for the discussion of other correlations).

Considering that existing data on binding energies does not allow to fully establish isovector properties of EDFs and make reliable predictions for masses of neutron-rich nuclei, it is important to have a closer look on NMP in order to see whether strict enforcement of NMP constraints could reduce theoretical uncertainties in isovector properties of EDFs and mass predictions for neutron-rich nuclei.

One way to do that is to see whether there is one-to-one correspondence between the differences in NMP of two functionals and the differences in their description of binding energies. Fig. 4 and Table III are created for such an analysis. The differences of the binding energies of several pairs of CEDFs are compared in Fig. 4; they are based on the results of the RHB calculations obtained in Ref. [10]. Table III summarizes the NMPs of employed functionals and the experimental/empirical ranges for the quantities of interest obtained in Ref. [1]. The binding energy per particle $E/A \sim -16$ MeV and the saturation density $\rho_0 \sim 0.15$ fm^{-3} represent well established properties of infinite nuclear matter. On the other hand, the incompressibility K_0 of symmetric nuclear matter, its symmetry energy J and the slope L_0 of symmetry energy at saturation density are characterized by substantial uncertainties (see Ref. [1] for details). Effective mass of the nucleon at the Fermi surface m^*/m is also poorly defined in experiment.

The smallest difference in the predictions of binding en-

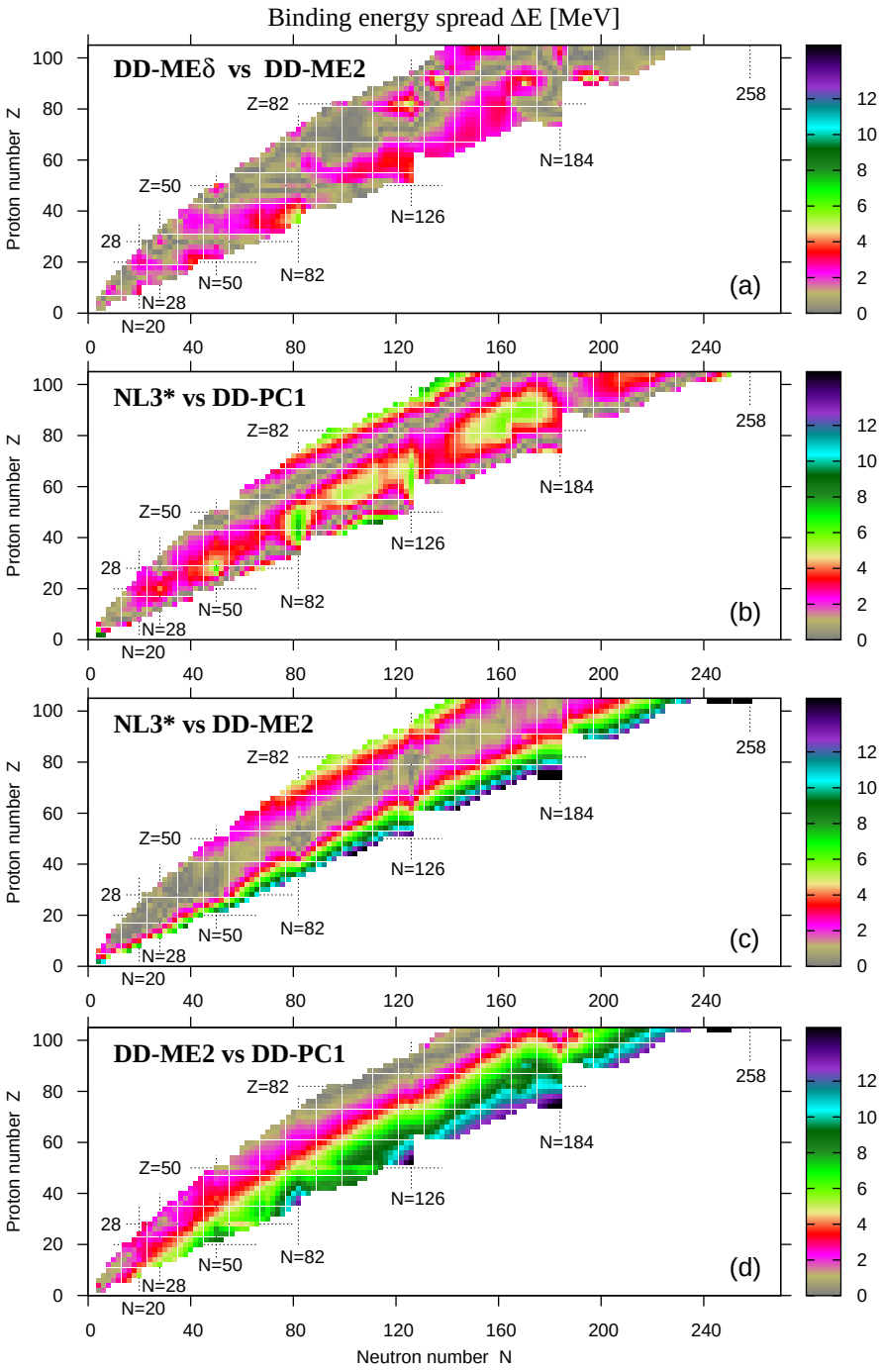

FIG. 4. (Color online) Binding energy spreads $\Delta E(Z,N)$ for the pairs of indicated functionals. All even-even nuclei between the two-proton and two-neutron drip lines are included in the comparison.

ergies exists for the DD-ME2/DD-MEδ pair of the functionals (Fig. 4a); for almost half of the $Z \leq 104$ nuclear landscape their predictions differ by less than 1.5 MeV and only in a few points of nuclear landscape the differences in binding energies of two functionals are close to 5 MeV. The NMPs of these two functionals are similar with some minor differences existing only for the incompressibility K_0 and Lorentz effective mass m^*/m (Table III). However, the similarity of NMP does not necessarily lead to similar predictions of binding energies. This is illustrated in Fig. 4d on the example of the pair of the DD-ME2 and DD-PC1 functionals for which substantial differences in the predictions exist for quite similar NMP (Table III).

Even more striking example is seen in Fig. 4b where the NL3*/DD-PC1 pair of the functionals, which are char-

TABLE III. Properties of symmetric nuclear matter at saturation: the density ρ_0, the energy per particle E/A, the incompressibility K_0, the symmetry energy J and its slope L_0, and the Lorentz effective mass m^*/m [38] of a nucleon at the Fermi surface. Top five lines show the values for indicated covariant energy density functionals, while bottom two lines show two sets (SET2a and SET2b) of the constraints on the experimental/empirical ranges for the quantities of interest defined in Ref. [1]. The CEDF values which are located beyond the limits of the SET2b constraint set are shown in bold.

CEDF	ρ_0 [fm^{-3}]	E/A [MeV]	K_0 [MeV]	J [MeV]	L_0 [MeV]	m^*/m
1	2	3	4	5	6	7
NL3* [18]	0.150	-16.31	258	**38.68**	**122.6**	0.67
DD-ME2 [19]	0.152	-16.14	251	32.40	49.4	0.66
DD-MEδ [21]	0.152	-16.12	219	32.35	52.9	0.61
DD-PC1 [20, 23]	0.152	-16.06	230	33.00	68.4	0.66
PC-PK1 [23]	0.154	-16.12	238	**35.6**	**113**	0.65
SET2a	~ 0.15	~ -16	190-270	25-35	25-115	
SET2b	~ 0.15	~ -16	190-270	30-35	30-80	

acterized by a substantial differences in the energy per particle (E/A), symmetry energy J and its slope L_0 (Table III), have significantly smaller differences in predicted binding energies as compared with above mentioned DD-ME2/DD-PC1 pair of the functionals. This is a consequence of a peculiar feature of the relative behavior of the binding energies of the NL3* and DD-PC1 functionals with increasing isospin which is clearly visible in Fig. 3. Note that the J and L_0 values of the NL3* functional are located outside the experimental/empirical ranges for these values defined in Ref. [1] (see Table III).

As mentioned in the introduction among the functionals for which global analysis of experimental binding energies exists only two, namely, FSUGold and DD-MEδ satisfy the majority of the NMP constraints. However, CEDFs FSUGold and DD-MEδ face significant problems in the description of finite nuclei. FSUGold is designed for neutron star applications in Ref. [39] and it is characterized by the largest rms deviations (6.5 MeV) from experiment for binding energies among all CEDF's the global performance of which is known [10]. At present, DD-MEδ is the most microscopic functional among all existing CEDFs; it relies on the pseudodata from *ab initio* calculations to determine density dependence of the meson-nucleon vertices so that only 4 parameters are fitted to the properties of finite nuclei. Although DD-MEδ provides quite reasonable description of binding energies (see Table II, Fig. 6 below and Refs. [10, 31]), it generates unrealistically low inner fission barriers in superheavy elements [40] and fails to reproduce octupole deformed nuclei in actinides [32].

The analysis of Refs. [10, 31, 32, 41, 42] clearly indicates that the CEDFs NL3*, DD-ME2, PC-PK1 and DD-PC1 represent better and well-rounded functionals as compared with FSUGold and DD-MEδ. They are able to describe not only ground state properties but also the properties of excited states [18–20, 41–46]. This is despite the fact that first three functionals definitely fail to describe some of the nuclear matter properties (see Table III and Ref. [1]). It is not clear whether that is also a case for DD-PC1 since it was not analyzed in Ref. [1]. As a result, one can conclude that the functionals, which provide good NMPs, do not necessary well describe finite nuclei. Such a possibility has already been mentioned in Ref. [1]. This is also in line with the results obtained for Skyrme EDFs [47] that the functionals reproducing NMP constraints cannot be necessarily expected to reproduce finite nuclei data, to which they were not fitted, with very high accuracy.

As a consequence, the NMP constraints do not allow to eliminate some of the CEDFs from the consideration and in this way to decrease the uncertainties in the predictions of binding energies of the neutron-rich nuclei and the position of two-neutron drip line; for a latter see also Sec. VIII in Ref. [10]. Considering substantial uncertainties in NMP (see Table III and Ref. [1]), it is clear that even the combination of their strict enforcement and the use of large data set on finite nuclei in the fitting protocols of new CEDFs will not lead to a substantial lowering or an elimination of the uncertainties in the predictions of binding energies of neutron-rich nuclei.

V. FINITE NUCLEI: THE ACCURACY OF THE DESCRIPTION OF THE GROUND STATE PROPERTIES AND ITS DEPENDENCE ON FITTING PROTOCOL

It is clear that the part of the difference in binding energy predictions is coming from the use of different data on finite nuclei in fitting protocols. For example, the binding energies of the "fitted" nuclei provide the normalization of the energy for the functional. Fitting protocols differ substantially (see Table I and Fig. 5) and it is important to understand how they affect the global results.

Almost exactly the same fitting protocols exist in the case of the NL3* and DD-ME2 functionals which were fitted to the same 12 spherical nuclei and the same "empirical" data on nuclear matter properties has been used in the fit [18, 19]. The only difference between them is the fact that 4 and 3 neutron skin thicknesses were used

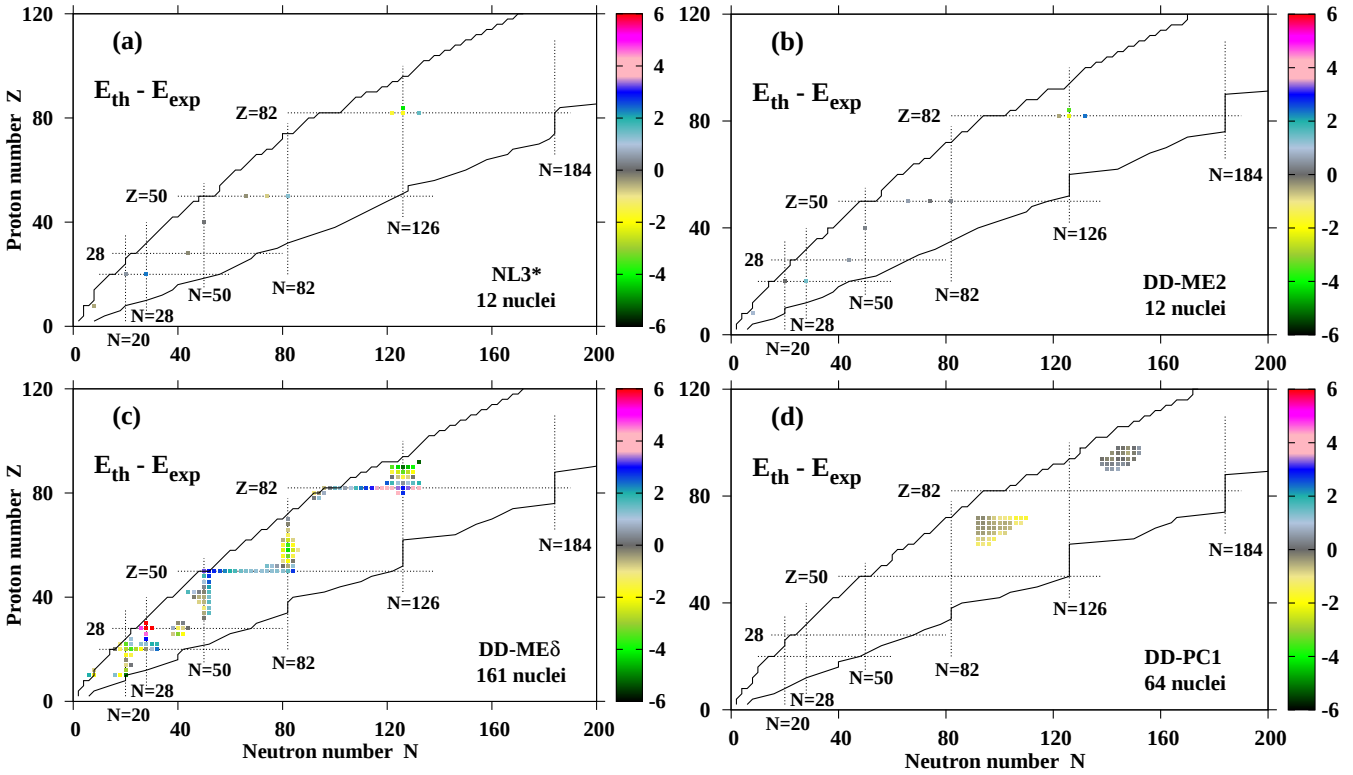

FIG. 5. (Color online) The nuclei (solid squares), shown in the (Z, N) plane, which were used in the fit of indicated CEDFs. Their total number is shown below the functional label. Magic shell closures are shown by dashed lines. The colors of the squares show the difference $E_{th} - E_{exp}$ between calculated and experimental binding energies. Two-proton and two-neutron drip lines of the indicated functional are shown by solid black lines.

in the fit of NL3* and DD-ME2 CEDFs, respectively. However, the impact of this difference is expected to be very small. Note that contrary to the DD-* functionals, NL3* CEDF does not have nonlinearities in the isovector channel. This leads to a relatively large values for the symmetry energy J and its slope L_0 at saturation (see Table III). As a result, the comparison of the calculated and experimental binding energies reveals that the DD-ME2 functional has better isovector properties than NL3* (Figs. 6a and b).

This also leads to somewhat better global reproduction of the charge radii in the DD-ME2 functional (see Table II and Figs. 7a and b). However, apart of few nuclei there is basically no difference in the description of experimental charge radii by NL3* and DD-ME2 for the $Z > 50$ nuclei (Fig. 8a) which suggests that the radii of these medium and heavy mass nuclei are not sensitive to non-linearities in the isovector channel. On the contrary, the Sn isotopes and lighter nuclei show much large sensitivity to the non-linearities in the isovector channel. This is an important feature which has to be taken into account when considering the use of future data on neutron-rich nuclei in the fit of new generation of the functionals. Note that for light nuclei beyond mean field effects could be more important than for heavy ones and this could be a possible reason for the deterioration of the accuracy of the description of the masses and radii in light systems as compared with heavy ones. It is also important to mention that despite the large similarities in the description of the charge radii in known nuclei by the CEDFs NL3* and DD-ME2 (Figs. 7a and b and Fig. 8a), there is a substantial increase of the differences in the predictions of the charge radii by these two CEDFs for the part of the nuclear chart roughly characterized by particle numbers $Z > 70$ and $N > 140$ (Fig. 9a).

The DD-* CEDFs show better isovector properties in the description of binding energies as compared with the NL3* one (Fig. 6). However, there are some important differences between the meson-exchange functionals (DD-ME2 and DD-MEδ) and point-coupling functional DD-PC1. They are the consequences of both the selection of the finite nuclei for the fitting protocol (Table I and Fig. 5) and the differences in underlying physics (meson exchange versus point coupling). Meson-exchange functionals are fitted to the spherical nuclei. As a result, deformed nuclei are typically underbound in these functionals (Fig. 6b and c). In contrast, DD-PC1 CEDF is fitted to the deformed nuclei and it reproduces the binding energies of such nuclei rather well especially in the rare-earth region and actinides (Fig. 5d). However, this functional tends to overbind spherical nuclei.

The differences in the underlying physics show them-

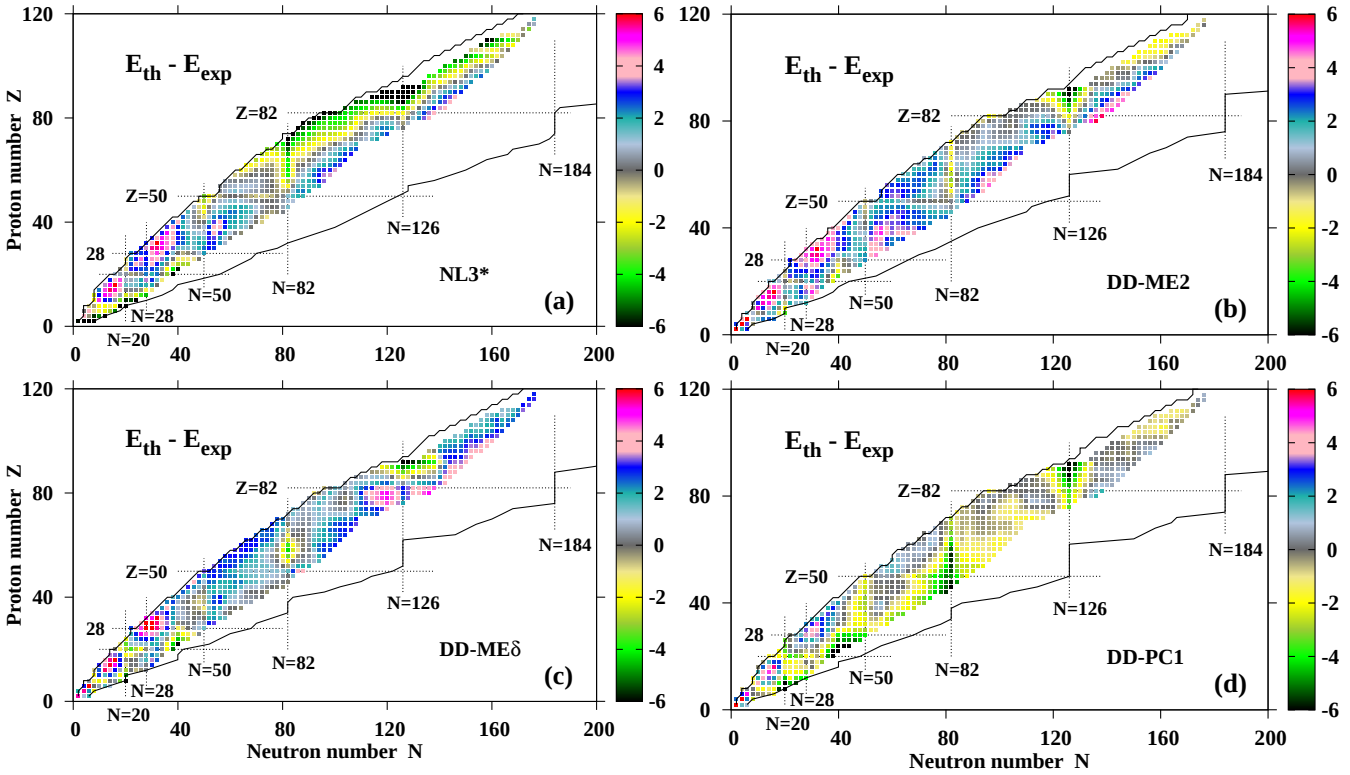

FIG. 6. (Color online) The differences $E_{th} - E_{exp}$ between calculated and experimental binding energies for the indicated CEDFs. The experimental data are taken from Ref. [28] and all 835 even-even nuclei, for which measured and estimated masses are available, are included. If $E_{th} - E_{exp} < 0$, the nucleus is more bound in the calculations than in experiment. Two-proton and two-neutron drip lines of the indicated functional are shown by solid black lines.

selves in different isovector properties of point coupling and meson exchange functionals. For example, similar description of experimental binding energies of neutron-deficient $72 < Z < 96$ nuclei is achieved in all DD-* functionals (Figs. 6b, c and d). However, neutron-rich $72 < Z < 96$ nuclei are underbound in the RHB calculations with CEDFs DD-ME2 and DD-MEδ (Figs. 6b and c) and overbound in the ones with DD-PC1 (Fig. 6d). Similar situation exists also for lighter nuclei in CEDF DD-PC1; neutron rich nuclei are overbound in the calculations while neutron deficient ones are either underbound or close to experiment. Thus, for DD-PC1 functional with increasing neutron number the binding energies increase faster in the calculations than in experiment across whole nuclear chart. The same trend for rate of binding energy changes is seen also in the CEDFs DD-ME2 and DD-MEδ for light nuclei (Figs. 6b and c); this is contrary to the situation in the heavy nuclei. Thus, the isovector dependence of binding energies is different in light and heavy nuclei in meson-exchange and point coupling functionals. Note that above discussed general trends are somewhat disturbed by local differences which emerge from the differences in the underlying shell structure.

Fig. 7 and Table II show the accuracy of the description of charge radii by density dependent functionals. One can see that CEDFs DD-ME2 and DD-PC1 provide comparable accuracy of the description of charge radii. On the other hand, the DD-MEδ functional provides worst description of the radii among considered functionals. Fig. 8b shows that apart of some light nuclei the DD-ME2 and DD-PC1 functionals provide almost the same description of charge radii across the nuclear chart. This is despite the fact that DD-PC1 functional has been defined without experimental data on charge radii in Ref. [20]. Figs. 8c and d show that the absolute majority of the spreads in charge radii for a set of four functionals is coming from the DD-MEδ functional; the next contributor to these spreads is the CEDF NL3* (Fig. 8).

However, global predictions for the charge radii are similar for density dependent functionals. Indeed, there are no global differences in the DD-ME2/DD-PC1 (Fig. 9c) and DD-MEδ/DD-ME2 (Fig. 9d) pairs of CEDFs similar to the ones observed in the NL3*/DD-ME2 (Fig. 9a) and NL3*/DD-PC1 (Fig. 9b) pairs for the part of the nuclear chart roughly characterized by particle numbers $Z > 70$ and $N > 140$. However, the local differences emerging from the underlying shell structure clearly exist. For example, substantial differences in charge radii seen at $Z \sim 90, N \sim 134$ for the DD-MEδ/DD-ME2 pair of the functionals (Fig. 9d) are due to inability of the CEDF DD-MEδ to describe octupole deformed nuclei in

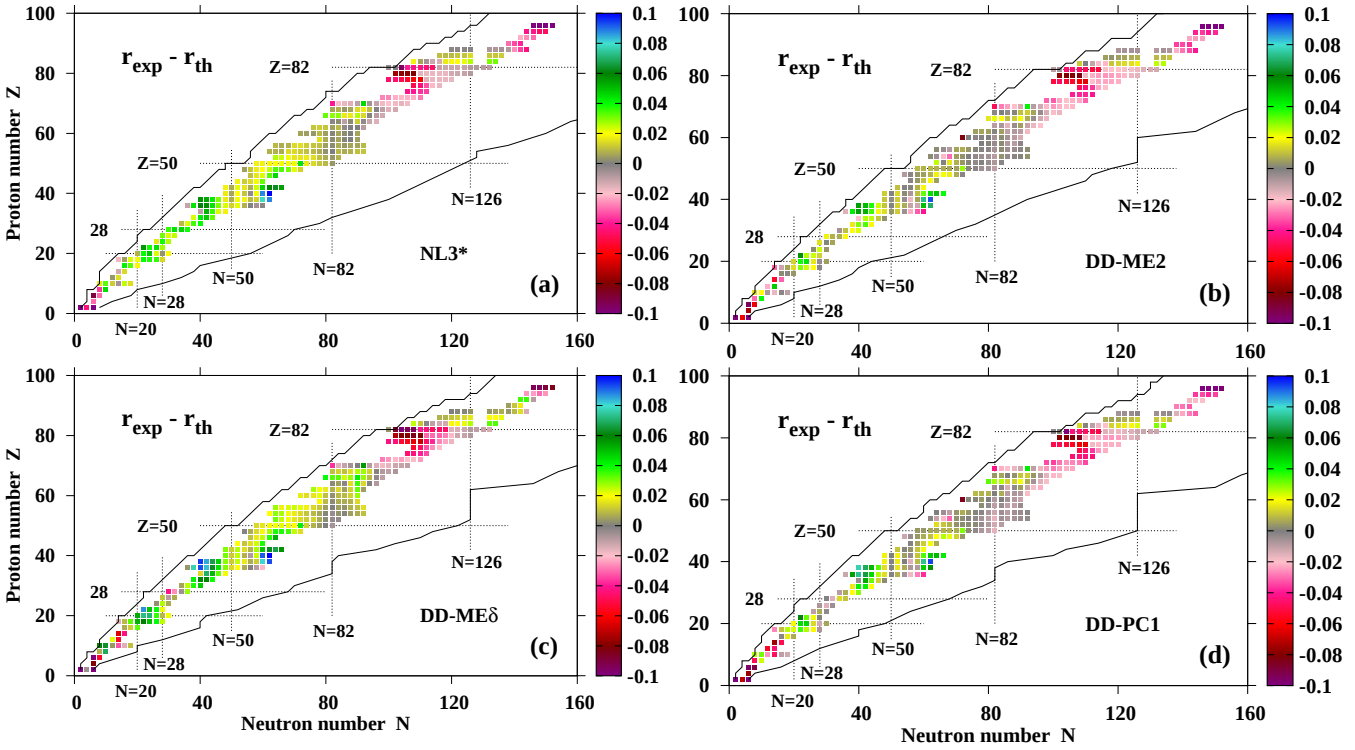

FIG. 7. (Color online) The difference between measured and calculated charge radii r_{ch} for indicated functionals. The experimental data are taken from Ref. [48]. Two-proton and two-neutron drip lines of the indicated functional are shown by solid black lines.

the actinides [32].

VI. GENERAL OBSERVATIONS

Based on the present analysis one could make the following observations:

- Fig. 4 shows that fastest increase of the differences in predicted binding energies of two functionals takes place in the direction which is perpendicular to the gray band of similar energies (or beta-stability line). These differences are due to (i) different isovector properties of these functionals and (ii) the differences in the selection of the input for the fitting protocols of these functionals.

  The differences in the NL3*/DD-ME2 pair of the functionals are mostly due to different isovector properties of compared functionals; they form smooth trends with almost no local fluctuations for the differences of both the binding energies (Fig. 4c) and charge radii (Fig. 9a). This is a consequence of the same fitting protocol used for both functionals which leads to a global similarity of their underlying single-particle structure.

  The differences in the input of the fitting protocols lead to local deviations from smooth trends which become especially visible in the case of the NL3*/DD-PC1 and DD-MEδ/DD-ME2 pairs of the functionals (see Figs. 4a and b for the differences of the binding energies and Figs. 9b and d for the differences of the charge radii). They are due to local differences in the underlying single-particle structure of the compared functionals.

  Thus, the selection of fitting protocol and in particular the selection of the information on finite nuclei has a direct influence and creates an imprint on the global performance of the CEDF.

- An important question is how much and which type of the data on finite nuclei are essential in the fitting protocols. Table II suggests that overdefined fitting protocols (such as DD-MEδ with 161 binding energies and 86 charge radii) do not offer any advantages as compared with the protocols which contain much less data since $\Delta E^{fit}_{rms} \approx \Delta E^{global}_{rms}$ and $\Delta(r_{ch})^{fit}_{rms} \approx \Delta(r_{ch})^{global}_{rms}$ for this functional. Note that DD-MEδ is only the functional with such properties; for all other functionals $\Delta E^{fit}_{rms} < \Delta E^{global}_{rms}$ and $\Delta(r_{ch})^{fit}_{rms} < \Delta(r_{ch})^{global}_{rms}$ (see Table II). The DD-PC1 CEDF [20] is an example of the functional which achieves good global description of charge radii (Table II) without any experimental data on charge radii in the fitting protocol (Table I). Curiously enough the addition of experimental data on charge radii to the fitting protocol of DD-PC1 could lead to the deterioration of

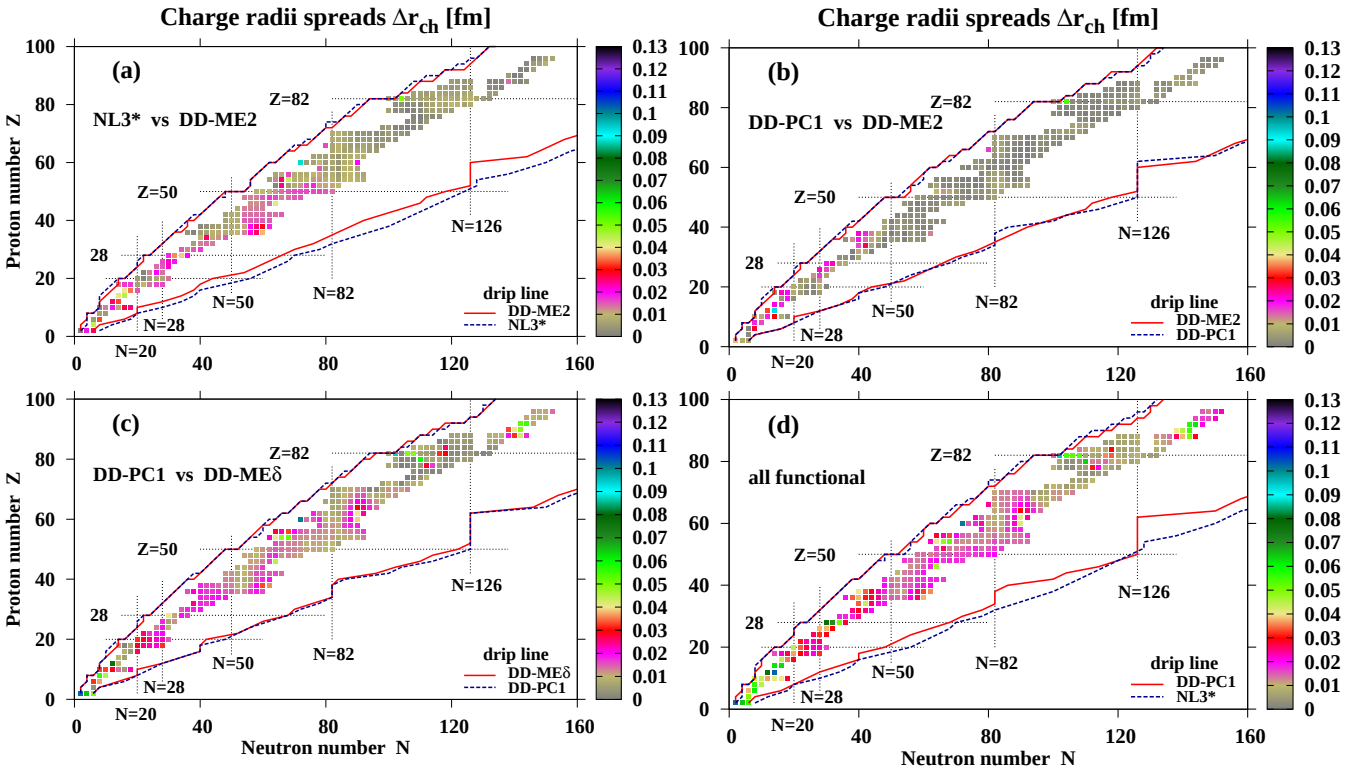

FIG. 8. (Color online) Charge radii spreads $\Delta r_{ch}(Z,N)$ as a function of proton and neutron number. $\Delta r_{ch}(Z,N) = |r_{ch}^{max}(Z,N) - r_{ch}^{min}(Z,N)|$, where $r_{ch}^{max}(Z,N)$ and $r_{ch}^{min}(Z,N)$ are the largest and smallest charge radii obtained either with indicated pairs of the CEDFs (panels (a)-(c)) or with four CEDFs (panel (d)) for the (Z,N) nucleus.

the accuracy of the description of charge radii since $\Delta(r_{ch})^{fit}_{rms} > \Delta(r_{ch})^{global}_{rms}$ (Table II). It turns out that the inclusion of very few but carefully selected experimental charge radii (like in the CEDF DD-ME2 with 9 charge radii) leads to a further but moderate increase of an accuracy of the global description of charge radii. The analysis of Table II also suggests that less than 100 data points on binding energies is sufficient for fitting protocols of a current generation of the CEDFs not aimed at the "mass table" quality description of binding energies.

- The variations of the differences in the predictions of the binding energies and the differences in the predictions of the charge radii of two functionals with proton and neutron numbers shown in Figs. 4 and 9 are not globally correlated.

- It is necessary to recognize that the binding energies are affected by the effects beyond mean field [25, 49, 50] which are not included in the current calculations. It was shown in Ref. [25] for the PC-PK1 functional that the inclusion of dynamic correlation energies (DCE) leads to a reduction of the rms-deviations for binding energies of 575 known even-even nuclei from 2.52 MeV (at the mean field level) to 1.14 MeV. DCE provides an additional binding and vary mostly in the region of $2.0 - 3.5$ MeV. It is expected that DCE will depend relatively weakly on the underlying functional (Ref. [25]). Thus, the accounting of DCE will not remove existing differences between the functionals seen in Figs. 1, 2, 3 and 4.

  On the other hand, the rms-deviations between experimental and calculated binding energies will be reduced for the DD-ME2 and DD-MEδ CEDFs when DCE are taken into account since these functionals typically underbind nuclei (see Figs. 6b and c). However, they will be increased for DD-PC1 since it provides good description of the binding energies of rare-earth nuclei and actinides at the mean field level (Fig. 6d). The inclusion of DCE will have probably overall neutral effect on the NL3* CEDF since it will improve the description of the binding energies of the $Z \leq 50$ nuclei but will lead to the decrease of the accuracy of the description of heavier nuclei (Fig. 6a).

- It is well known that high-density behaviour of EOS has little influence on the description of low-energy nuclear structure data [20]. For the first time our studies confirm this fact on a global scale in the framework of CDFT. Indeed, the functionals which have stiff equation of state (NL3*, DD-ME2 and PC-PK1) are still accurate in the description of the ground state properties. The current analysis

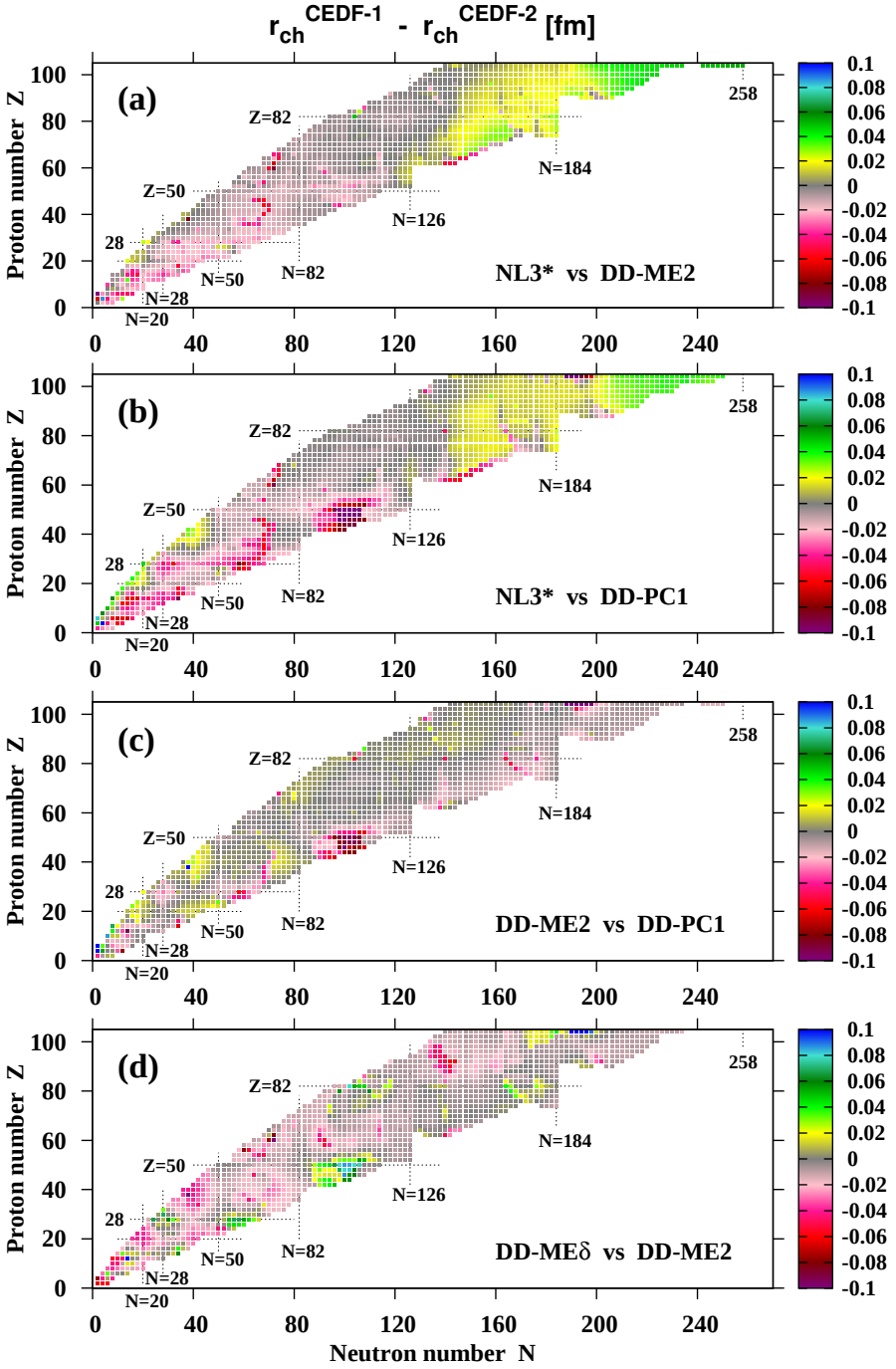

FIG. 9. (Color online) The difference $r_{ch}^{CEDF-1}(Z,N) - r_{ch}^{CEDF-2}(Z,N)$ in the charge radii predicted by two indicated CEDFs. The second functional in the label "CEDF-1 vs CEDF-2" indicates the reference functional. All even-even nuclei between the two-proton and two-neutron drip lines are included in the comparison.

clearly indicates that apart of the NL3* functional, which does not have a good reproduction of the isospin trends for the binding energies, the remaining functionals are quite comparable at the mean field level. Considering similar (as compared with experiment) initial starting mean field solutions for CEDFs DD-ME2, DD-MEδ and PC-PK1 (see Fig. 6 and Fig. 3 in Ref. [25]) and weak dependence of dynamic correlation energies on the functional, it is reasonable to expect that CEDFs DD-ME2 and DD-MEδ will have similar to PC-PK1 rms-deviations for binding energies ($\Delta E_{rms}^{global} \sim 1.14$ MeV [25]) when DCEs are included. Thus, the functionals with $J \sim 32$ MeV and $L_0 \sim 50$ MeV (DD-ME2 and DD-MEδ) and $J = 35.6$ MeV and $L_0 = 113$ MeV (PC-PK1) provide quite compara-

ble global description of the binding energies. For the first time in CDFT, this confirms on a global scale earlier observations that nuclear binding energies represent poor isovector indicators [2].

The slope of symmetry energy L_0, which is good isovector indicator, is not well defined at present (see Table III and Ref. [1]). However, it strongly correlates with the size of neutron skin thickness so that CEDFs NL3* and PC-PK1 predict larger neutron skin than DD-* functionals (see Sec. X in Ref. [10]). At present, the uncertainties in experimental definition of neutron skin still exist. However, there is a hope that the PREX-II experiment aimed at the measurement of neutron radii in ^{208}Pb will put a stricter constraint on the density dependence of the symmetry energy (the L_0 parameter) (Ref. [6]).

- A common trend of the discrepancies between calculated and experimental charge radii is clearly seen for all functionals in Fig. 7. The RHB calculations typically underestimate the radii in the $Z \leq 50$ nuclei, rather well reproduce them in the rare-earth region and overestimate them in the actinides. This trend is based on the consideration which excludes neutron deficient nuclei in the lead and krypton regions; they are characterized by shape coexistence which cannot be described at the mean field level (see Sec. X of Ref. [10] for a discussion of these nuclei). It remains to be seen to which extent this trend is due to the use of the equation

$$r_{ch} = \sqrt{< r^2 >_p + 0.64}\ fm, \tag{3}$$

for charge radii. The factor 0.64 accounts for the finite-size effects of the proton. This equation is used in the CDFT calculations [51, 52] but it ignores small contributions to the charge radius originating from the electric neutron form factor and electromagnetic spin-orbit coupling [53, 54] as well as the corrections due to the center-of-mass motion.

VII. CONCLUSIONS

The question of how strictly nuclear matter constraints have to be imposed and which values have to be used for the definition of covariant energy density functionals still remains not fully answered. Definitely, the equation of state relating pressure, energy density, and temperature at a given particle number density is essential for modeling neutron stars, core-collapse supernovae, mergers of neutron stars and the processes (such as nucleosynthesis) taking places in these environments. However, there are substantial experimental/empirical/model uncertainties in the definition of the NMP constraints.

In addition, the properties of finite nuclei are defined by the underlying shell structure which depends sensitively on the single-particle features [7, 8, 31]. As a consequence, we are facing the situation in which the functionals which are coming close to satisfying all NMP constraints perform quite poorly in the description of finite nuclei. This was exemplified by the FSUGold and DD-MEδ functionals. The former provides the worst rms-deviations in global description of binding energies [9, 10], while the latter fails to reproduce octupole deformed actinides [31] and predicts too low fission barriers in superheavy nuclei [40] so that their existence could be questioned. On the other hand, the functionals which fail to reproduce the NMP constraints suggested in Ref. [1] such as NL3* and PC-PK1 are able to reproduce reasonably well the ground state properties of finite nuclei, such as binding energies and charge radii, fission barriers [41, 45, 55], rotating nuclei [42, 44] and the energies of the single-particle states in spherical [56, 57] and deformed nuclei [43, 58].

The correlations between global description of the binding energies and nuclear matter properties of the underlying functionals have been discussed based on the results of recent assessment of global performance of covariant energy density functionals presented in Refs. [10, 16, 22]. It was concluded that the strict enforcement of the limits on the nuclear matter properties defined in Ref. [1] will not necessary (i) lead to the functionals with good description of binding energies or other ground and excited state properties or (ii) substantially reduce the uncertainties in the description of neutron-rich systems. This is very likely due to to the mismatch of phenomenological content, existing in all modern functionals, related to nuclear matter physics and the physics of finite nuclei; the latter being strongly affected by underlying shell effects.

VIII. ACKNOWLEDGMENTS

This material is based upon work supported by the U.S. Department of Energy, Office of Science, Office of Nuclear Physics under Award Number DE-SC0013037. We would like to express our deep graditude to D. Ray and P. Ring, who contributed to Ref. [10] the numerical results of which were used in this manuscript.

[1] M. Dutra, O. Lourenco, S. S. Avancini, B. V. Carlson, A. Delfino, D. P. Menezes, C. Providencia, S. Typel, and J. R. Stone, Phys. Rev. C **90**, 055203 (2014).

[2] W. Nazarewicz, P.-G. Reinhard, W. Satula, and D. Vretenar, Eur. Phys. J. A **50**, 20 (2014).
[3] J. M. Pearson, N. Chamel, A. F. Fantina, and S. Goriely, Eur. Phys. J. **A50**, 43 (2014).
[4] J. Piekarewicz, Eur. Phys. J. **A50**, 25 (2014).
[5] G. Colo, U. Gard, and H. Sagawa, Eur. Phys. J. **A50**, 20 (2014).
[6] C. J. Horowitz, K. S. Kumar, and R. Michaels, Eur. Phys. J. **A50**, 48 (2014).
[7] M. Bender, P.-H. Heenen, and P.-G. Reinhard, Rev. Mod. Phys. **75**, 121 (2003).
[8] D. Vretenar, A. V. Afanasjev, G. A. Lalazissis, and P. Ring, Phys. Rep. **409**, 101 (2005).
[9] P.-G. Reinhard and B. K. Agrawal, Int. Jour. Mod. Phys. **E20**, 1379 (2011).
[10] S. E. Agbemava, A. V. Afanasjev, D. Ray, and P. Ring, Phys. Rev. C **89**, 054320 (2014).
[11] M. Dutra, O. Lourenco, and D. P. Menezes, Phys. Rev. C **93**, 025806 (2016).
[12] P. B. Demorest, T. Pennucci, S. M. Ransom, M. S. E. Roberts, and J. W. T. Hessels, Nature **467**, 1081 (2010).
[13] J. Antoniadis, P. C. C. Freire, N. Wex, T. M. Tauris, R. S. Lynch, M. H. van Kerkwijk, M. Kramer, C. Bassa, V. S. Dhillon, T. Driebe, J. W. T. Hessels, V. M. Kaspi, V. I. Kondratiev, N. Langer, T. R. Marsh, M. A. McLaughlin, T. T. Pennucci, S. M. Ransom, I. H. Stairs, J. van Leeuwen, J. P. W. Verbiest, and D. G. Whelan, **340**, 448 (2013).
[14] D. Chatterjee and I. Vidaña, Eur. Phys. J. **A52**, 29 (2016).
[15] J. Erler, N. Birge, M. Kortelainen, W. Nazarewicz, E. Olsen, A. M. Perhac, and M. Stoitsov, Nature **486**, 509 (2012).
[16] A. V. Afanasjev, S. E. Agbemava, D. Ray, and P. Ring, Phys. Lett. B **726**, 680 (2013).
[17] M. R. Mumpower, R. Surman, G. C. McLaughlin, and A. Aprahamian, Prog. Part. Nucl. Phys. **86**, 86 (2016).
[18] G. A. Lalazissis, S. Karatzikos, R. Fossion, D. P. Arteaga, A. V. Afanasjev, and P. Ring, Phys. Lett. **B671**, 36 (2009).
[19] G. A. Lalazissis, T. Nikšić, D. Vretenar, and P. Ring, Phys. Rev. C **71**, 024312 (2005).
[20] T. Nikšić, D. Vretenar, and P. Ring, Phys. Rev. C **78**, 034318 (2008).
[21] X. Roca-Maza, X. Viñas, M. Centelles, P. Ring, and P. Schuck, Phys. Rev. C **84**, 054309 (2011).
[22] A. V. Afanasjev, S. E. Agbemava, D. Ray, and P. Ring, Phys. Rev. C **91**, 014324 (2015).
[23] P. W. Zhao, Z. P. Li, J. M. Yao, and J. Meng, Phys. Rev. C **82**, 054319 (2010).
[24] Q. S. Zhang, Z. M. Niu, Z. P. Li, J. M. Yao, and J. Meng, Frontiers of Physics **9**, 529 (2014).
[25] K. Q. Lu, Z. X. Li, Z. P. Li, J. M. Yao, and J. Meng, Phys. Rev. C **91**, 027304 (2015).
[26] A. Akmal, V. R. Pandharipande, and D. G. Ravenhall, Phys. Rev. C **58**, 1804 (1998).
[27] Z. H. Li and H.-J. Schulze, Phys. Rev. C **78**, 028801 (2008).
[28] M. Wang, G. Audi, A. H. Wapstra, F. G. Kondev, M. MacCormick, X. Xu, and B. Pfeiffer, Chinese Physics **C36**, 1603 (2012).
[29] H. Schatz, private communication, see also https://groups.nscl.msu.edu/frib/rates/fribrates.html (2014).
[30] J. D. McDonnell, N. Schunck, D. Higdon, J. Sarich, S. M. Wild, and W. Nazarewicz, Phys. Rev. Lett. **114**, 122501 (2015).
[31] S. E. Agbemava, A. V. Afanasjev, T. Nakatsukasa, and P. Ring, Phys. Rev. C **92**, 054310 (2015).
[32] S. E. Agbemava, A. V. Afanasjev, and P. Ring, Phys. Rev. C **93**, 044304 (2016).
[33] P.-G. Reinhard and W. Nazarewicz, arXiv: nucl-th/1601.06324v1 (2016).
[34] F. J. Fattoyev and J. Piekarewicz, Phys. Rev. C **84**, 064302 (2011).
[35] X. Roca-Maza, N. Paar, and G. Colò, J. Phys. G **42**, 034033 (2015).
[36] P. G. Reinhard and W. Nazarewicz, Phys. Rev. C **81**, 051303(R) (2010).
[37] J. Piekarewicz, B. K. Agrawal, G. Colò, W. Nazarewicz, N. Paar, P.-G. Reinhard, X. Roca-Maza, and D. Vretenar, Phys. Rev. C **85**, 041302 (2012).
[38] M. Jaminon and C. Mahaux, Phys. Rev. C **40**, 354 (1989).
[39] B. G. Todd-Rutel and J. Piekarewicz, Phys. Rev. Lett. **95**, 122501 (2005).
[40] S. E. Agbemava, A. V. Afanasjev, T. Nakatsukasa, and P. Ring, (in preparation).
[41] H. Abusara, A. V. Afanasjev, and P. Ring, Phys. Rev. C **82**, 044303 (2010).
[42] A. V. Afanasjev and O. Abdurazakov, Phys. Rev. C **88**, 014320 (2013).
[43] A. V. Afanasjev and S. Shawaqfeh, Phys. Lett. B **706**, 177 (2011).
[44] J. Meng, J. Peng, S.-Q. Zhang, and P.-W. Zhao, Front. Phys. **8**, 55 (2013).
[45] B.-N. Lu, J. Zhao, E.-G. Zhao, and S.-G. Zhou, Phys. Rev. C **89**, 014323 (2014).
[46] V. Prassa, T. Nikšić, G. A. Lalazissis, and D. Vretenar, Phys. Rev. C **86**, 024317 (2012).
[47] P. D. Stevenson, P. M. Goddard, J. R. Stone, and M. Dutra, AIP Conf. Proc. **1529**, 269 (2013).
[48] I. Angeli and K. P. Marinova, At. Data Nucl. Data Tables **99**, 69 (2013).
[49] M. Bender, G. F. Bertsch, and P.-H. Heenen, Phys. Rev. C **73**, 034322 (2006).
[50] S. Goriely, N. Chamel, and J. M. Pearson, Phys. Rev. Lett. **102**, 152503 (2009).
[51] P. Ring, Prog. Part. Nucl. Phys. **37** (1996).
[52] L. Geng, H. Toki, and J. Meng, Prog. Theor. Phys. **113**, 785 (2005).
[53] W. Bertozzi, J. Friar, J. Heisenberg, and J. W. Negele, Phys. Lett. B **41**, 408 (1972).
[54] M. Nishimura and D. W. L. Sprung, Prog. Theor. Phys. **77**, 781 (1987).
[55] H. Abusara, A. V. Afanasjev, and P. Ring, Phys. Rev. C **85**, 024314 (2012).
[56] E. V. Litvinova and A. V. Afanasjev, Phys. Rev. C **84**, 014305 (2011).
[57] A. V. Afanasjev and E. Litvinova, Phys. Rev. C **92**, 044317 (2015).
[58] J. Dobaczewski, A. V. Afanasjev, M. Bender, L. M. Robledo, and Y. Shi, Nucl. Phys. A **944**, 388 (2015).